JACS
JOURNAL OF THE AMERICAN CHEMICAL SOCIETY
Article
pubs.acs.org/JACS

Boosting Power Conversion Efficiencies of Quantum-Dot-Sensitized Solar Cells Beyond 8% by Recombination Control

Ke Zhao,[†,#] Zhenxiao Pan,[†,#] Iván Mora-Seró,[‡,#] Enrique Cánovas,[¶] Hai Wang,[¶,∥] Ya Song,[†] Xueqing Gong,[†] Jin Wang,[†] Mischa Bonn,[¶] Juan Bisquert,[‡,§] and Xinhua Zhong*[,†]

[†]Key Laboratory for Advanced Materials, School of Chemistry and Molecular Engineering, East China University of Science and Technology, Shanghai 200237, China

[‡]Photovoltaic, Optoelectronic Devices Group, Department de Física, Universitat Jaume I, 12071 Castelló, Spain

[¶]Max Planck Institute for Polymer Research, Ackermannweg 10, 55128 Mainz, Germany

[∥]Graduate School Material Science in Mainz, University of Mainz, Staudingerweg 9, 55099 Mainz, Germany

[§]Department of Chemistry, Faculty of Science, King Abdulaziz University, Jeddah 22254, Saudi Arabia

Supporting Information

ABSTRACT: At present, quantum-dot-sensitized solar cells (QDSCs) still exhibit moderate power conversion efficiency (with record efficiency of 6−7%), limited primarily by charge recombination. Therefore, suppressing recombination processes is a mandatory requirement to boost the performance of QDSCs. Herein, we demonstrate the ability of a novel sequential inorganic ZnS/SiO_2 double layer treatment onto the QD-sensitized photoanode for strongly inhibiting interfacial recombination processes in QDSCs while providing improved cell stability. Theoretical modeling and impedance spectroscopy reveal that the combined ZnS/SiO_2 treatment reduces interfacial recombination and increases charge collection efficiency when compared with conventional ZnS treatment alone. In line with those results, subpicosecond THz spectroscopy demonstrates that while QD to TiO_2 electron-transfer rates and yields are insensitive to inorganic photoanode overcoating, back recombination at the oxide surface is strongly suppressed by subsequent inorganic treatments. By exploiting this approach, $CdSe_xTe_{1-x}$ QDSCs exhibit a certified record efficiency of 8.21% (8.55% for a champion cell), an improvement of 20% over the previous record high efficiency of 6.8%, together with an additional beneficial effect of improved cell stability.

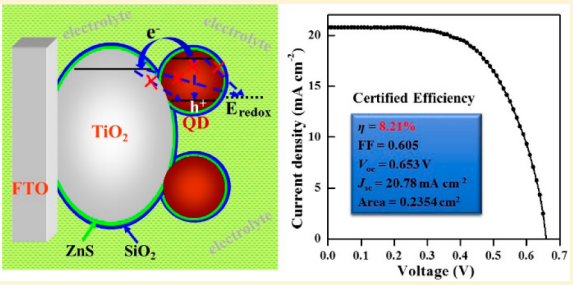

INTRODUCTION

Semiconductor quantum dots (QDs) are extremely appealing building blocks for optoelectronic applications. In particular, exploiting QDs as solar harvesters constitutes a promising approach toward low-cost third-generation solar cells owing to their band gap tunability, high absorption coefficient, solution processability, and multiple exciton generation possibilities.[1−6] Despite these advantages, QD solar cells still exhibit moderate power conversion efficiencies (PCE) of 6−8%, limited primarily by charge recombination.[3,4,7] This limitation is observed independent of the configuration of QD solar cells, i.e., for both depleted heterojunction solar cells,[8−10] and sensitized configurations in QD-sensitized solar cells (QDSCs).[11−14] Up to date, published best QD depleted heterojunction solar cells achieved 8.55% efficiency (1.37 mm^2 area),[8] while certified and noncertified PCEs for electrolyte and solid-state-based QDSCs lie at 6.82% (23.67 mm^2 area)[11] and 7.5% (16 mm^2 area),[14] respectively. The PCE improvement for QDSCs has been achieved primarily by two distinct approaches: on the one hand, the improvement of fill factor (FF) using counter electrodes especially adapted to polysulfide electrolyte, mainly Cu_2S,[15−19] and on the other hand the enhancement of short-circuit current, J_{sc}, achieved by increasing the light-harvesting capability through the adoption of near-infrared adsorption QD sensitizers or the modification of sensitization method (i.e. by extending light absorption range and/or QD loading amount).[20−25] Further improvement of QDSC efficiencies requires the improvement of the open-circuit potential, V_{oc}, by the use of a new redox system or by an accurate control of parasitic recombination processes.[26−29] This report focuses on this last consideration.

Interfacial recombination constitutes one of the main factors limiting the performance of sensitized solar cells.[30] Suppressing recombination in QDSCs is even more critical due to the potential contribution of defect states in QDs (notably at their surface) and the inherent lower sensitizer loading on the oxide photoanode (increasing oxide/electrolyte interface area).[7,31] To suppress charge recombination in sensitized cells, overcoating the mesoporous oxide electrode with a thin wide band gap inorganic barrier layer have been extensively explored in both QD and dye-sensitized solar cells.[32−43]

Received: March 11, 2015

DOI: 10.1021/jacs.5b01946
J. Am. Chem. Soc. XXXX, XXX, XXX−XXX

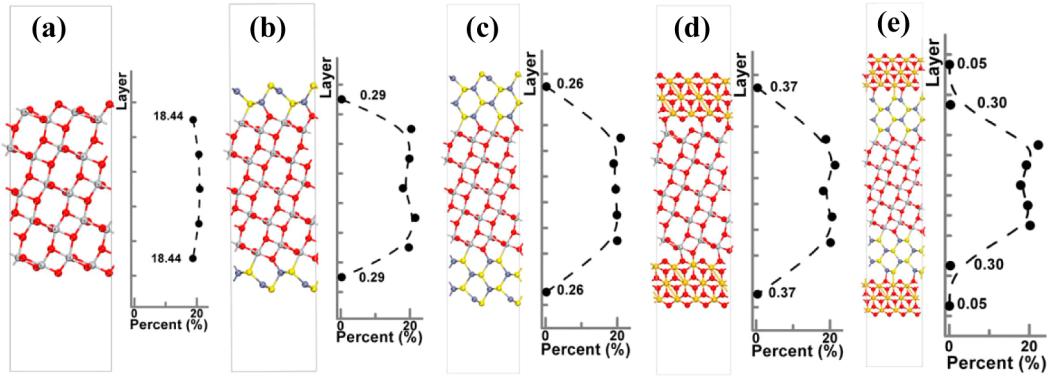

Figure 1. Calculation of DOS for electrodes with different coatings: (a) clean TiO_2(101), and the surfaces coated with (b) 1 ML ZnS, (c) 2 ML ZnS, (d) 3 ML SiO_2, and (e) 2 ML ZnS and 3 ML SiO_2. O atoms in red, Ti in gray, S in yellow, Zn in gray blue, and Si in gold. The calculated relative amount of empty states within the 1 eV window above the CB minimum of different layers is plotted in percentage beside the corresponding slabs (points).

Although ZnS is the most popular photoanode coating material for preventing interfacial recombination in QDSCs,[36−39] other materials such as TiO_2,[40] Al_2O_3,[41] SiO_2,[42] or MgO[43] have also been reported. All these inorganic overcoating layers basically act as energy barriers to prevent recombination of photogenerated electrons in the nanostructured oxide with holes residing in hole conductor (e.g., electrolyte).[32−43] The barrier treatment can be included before or after sensitization. Note that placing it before or after will affect the electron-transfer (ET) rate to the oxide or the hole-transfer rate to the electrolyte, respectively. In any case, the treatment after sensitization provides a path for passivating the QDs and increasing cell stability (e.g., by protecting QDs from potential corrosion by the electrolyte). Despite the great success of the surface coating in QDSCs, several works suggest that further reduction in recombination can be achieved beyond the reduction obtained with a single barrier passivation. For example, combination of ZnS coating with different dipolar molecules absorbed on the surface of TiO_2 has been reported to improve the performance of QDSCs.[44,45]

Herein, we demonstrate that a novel ZnS/SiO_2 double barrier coating treatment, sequentially deposited after QD sensitization on photoanode, reduces substantially the recombination in QDSCs (for both CdSe- and $CdSe_xTe_{1-x}$-based cell devices) while increasing their stability. The nature of this treatment is analyzed theoretically, and its impact on charge transport and transfer at the QD/oxide interface scrutinized by impedance and THz spectroscopy. Finally QD-sensitized solar cells with efficiencies beyond 8% are reported, representing a 20% improvement over current QDSCs approaches. In addition, an improvement in solar cell stability is reported when comparing our novel double layer treatment with conventional single architectures.

RESULTS AND DISCUSSION

Theoretical Calculations. In order to unravel the passivating effect of inorganic treatments onto the photoanode, anatase TiO_2 coated with ZnS and SiO_2 layers (Figure 1) has been studied using first-principles density functional theory (DFT) calculations corrected by a Hubbard-U term (DFT + U), where U = 6.2 eV was applied to its Ti 3d states (see Supporting Information, SI, for details).[46,47]

In Figure 1a−e, we show the conduction band (CB) density of states (DOS), consisting of empty electronic states distributed in the bulk and surface layer. We calculate the relative amount of empty states distributed at different spatial locations on an untreated TiO_2 slab with those coated with single and double barriers treatment (with 1 monolayer (ML) of ZnS, 2 ML ZnS, 3 ML SiO_2, and 2 ML ZnS + 3 ML SiO_2). From the calculation we resolve that a ZnS layer deposition onto TiO_2 (101) (Figure 1b) can achieve oxide surface passivation by forming well-ordered Zn−O and S−Ti bonds that saturate all the dangling bonds at the oxide surface (coordinate-unsaturated O_{2c} and Ti_{5c}). Moreover, the double barrier system with SiO_2 on top of the ZnS (Figure 1e) also forms compact Si−S, O−Zn bonds at the SiO_2/ZnS interface that terminate all the exposed Zn and S surface atoms. However, for TiO_2 (101) coated directly by SiO_2 (Figure 1d), distorted Si−O and Ti−O bonds appear at the interface, and only partial Ti_{5c} and O_{2c} dangling bonds are saturated as shown in Figure S1.

A quantitative analysis of the distribution of empty states clearly shows that (i) bare TiO_2 gives rise to a large amount of empty states (~18%) at the exposed surfaces (Figure 1a); (ii) ZnS and SiO_2 coatings reduce efficiently, by 2 orders of magnitude, the density of surface states to 0.29% (0.26% for 2 ML ZnS) and 0.37%, respectively (Figure 1b−d); and (iii) SiO_2 layer on top of ZnS can further reduce, by an additional order of magnitude, the exposed DOS to an overall value as low as 0.05% (Figure 1e). The calculated DOS is shown in Figure S2. These theoretical calculations of the structural and electronic properties of differently coated TiO_2 surfaces clearly show the capability of ZnS/SiO_2 coating to strongly reduce electron dissipation at the outermost surface, suggesting that the double coating treatment can be used to control recombination in QDSCs. In addition, the SiO_2 layer plays a very important colateral effect providing a path for enhancing solar cell stability, inhibiting photocorrosion as discussed below.

Structural Characterization. Following the results derived from the theoretical analysis, we developed different batches of solar cells in order to evaluate the strength of the ZnS/SiO_2 double coating approach. We employed $CdSe_{0.65}Te_{0.35}$ (simplified as CdSeTe henceforth) QDs with an absorption onset at ~800 nm, from which over 6% efficiency has been reported in previous literature.[23,48] The QDs were prepared and subsequently immobilized on TiO_2 film electrodes via capping ligand induced self-assembly approach, using thioglycolic acid (TGA)-capped water-soluble QDs according to

DOI: 10.1021/jacs.5b01946
J. Am. Chem. Soc. XXXX, XXX, XXX−XXX

our previously developed method.[22,48] Similar to previous reports,[11,22,28] this sensitization method produces a high QD loading, and the corresponding TEM image for the QD-sensitized TiO_2 film electrode was shown in Figure S3. QDSCs just prepared with QD-sensitized photoanode and no further inorganic layer coating will be denoted hereafter as plain QD samples. In addition, CdSeTe QD-sensitized electrodes were also coated with ZnS by different number of successive ionic absorption and reaction (SILAR) cycles (denoted hereafter as *n*ZnS, where "*n*" is the number of SILAR cycles) in methanol media. Finally samples with a double coating of 4ZnS/SiO_2 (i.e., first 4ZnS followed by a SiO_2 coating layer), as schematically shown in Figure 2a, have been also prepared.

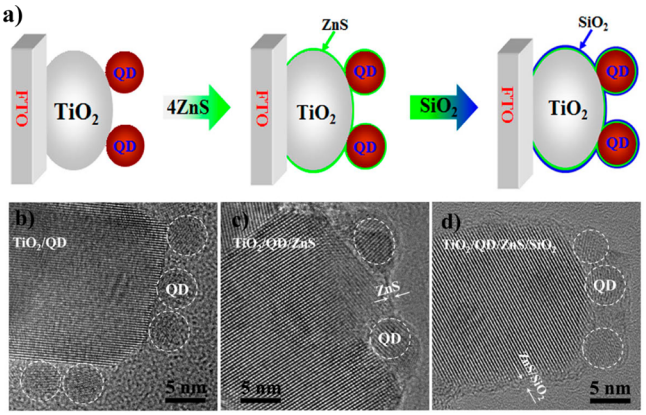

Figure 2. Scheme and micrographs of sensitized electrodes with and without barrier coating. (a) Schematic showing the sequential overcoating of ZnS and SiO_2 thin layer around the QD-sensitized TiO_2 film electrode. The corresponding HRTEM images (b) for TiO_2 electrodes just sensitized with CdSeTe QDs, (c) 4ZnS layer overcoated, and (d) 4ZnS/SiO_2 overcoated CdSeTe QD-sensitized TiO_2 film electrodes. For clarity, the ZnS, SiO_2 overlayers are indicated by arrows, and the dashed circles were artificially added around QDs.

Detailed procedure is described in the Experimental Section. The successful overcoating of ZnS and SiO_2 onto QD-sensitized TiO_2 electrode is evident from the high-resolution transmission electronic micrograph (HRTEM) images as shown in Figure 2b–d, which demonstrate clearly the deposition of a conformal ZnS layer with average thickness of ~0.7 nm and a ZnS/SiO_2 thin layer (with total thickness of ~1.5 nm) on the exposed surface of both TiO_2 and CdSeTe QD as highlighted by the arrows in the images.

To further confirm the observed amorphous layers around the sensitized photoanode is actually the claimed ZnS and SiO_2, X-ray photoelectron spectrum (XPS) measurements were performed on samples of the CdSeTe QD-sensitized TiO_2 mesoporous film with and without ZnS, ZnS/SiO_2 overlayer. Unlike the XPS spectrum of the reference TiO_2/QD sample, Zn signal appears in that of TiO_2/QD/ZnS sample (Figure 3c), while both Zn and Si signals appear in that of TiO_2/QD/ZnS/SiO_2 sample (Figure 3c,d). This clearly confirms the presence of ZnS, and ZnS/SiO_2 layers in the specified samples, respectively. Furthermore, the intensity of Ti and Cd signals is reduced sequentially in TiO_2/QD/ZnS and TiO_2/QD/ZnS/SiO_2 samples as compared with those in the reference TiO_2/QD sample (Figure 3a,b). Similarly, the intensity of Zn signal in TiO_2/QD/ZnS/SiO_2 is significantly reduced in comparison with that in TiO_2/QD/ZnS (Figure 3c). This observed signal attenuation is stemmed from the blocking effect by the ZnS,

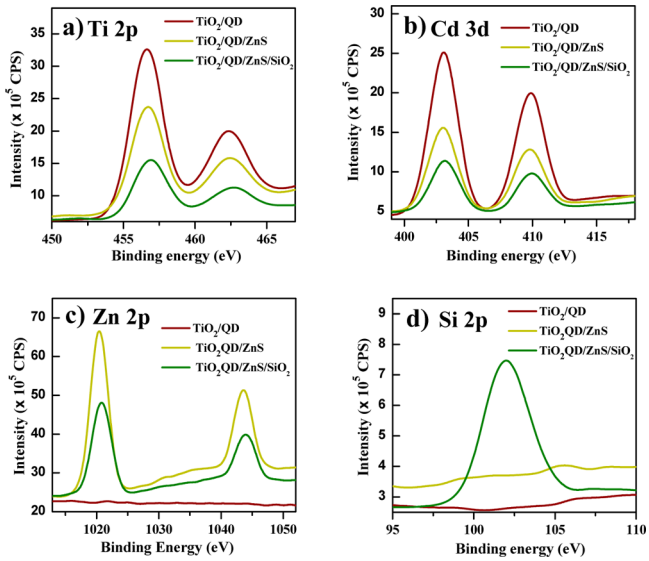

Figure 3. X-photoelectron spectra of the plain photoanode TiO_2/QD, ZnS overcoated photoanode TiO_2/QD/ZnS and ZnS/SiO_2 overcoated photoanode TiO_2/QD/ZnS/SiO_2: (a) Ti 2p, (b) Cd 3d, (c) Zn 2p, and (d) Si 2p signals.

and ZnS/SiO_2 layer around the sensitized photoanode due to the definite detection deepness in the XPS technique. Therefore, the coverage of ZnS on the TiO_2/QD and SiO_2 on the TiO_2/QD/ZnS surface is evident.

Photovoltaic Performance. As illustrated in Figure 4a, the absorbance of QD-sensitized electrodes increases only slightly in the region of 500–750 nm after coating, indicating that ZnS and ZnS/SiO_2 coatings have a minor influence on the light harvesting capability of the cells, in agreement with previous reports.[37,38] Moreover, complete solar cells were constructed by

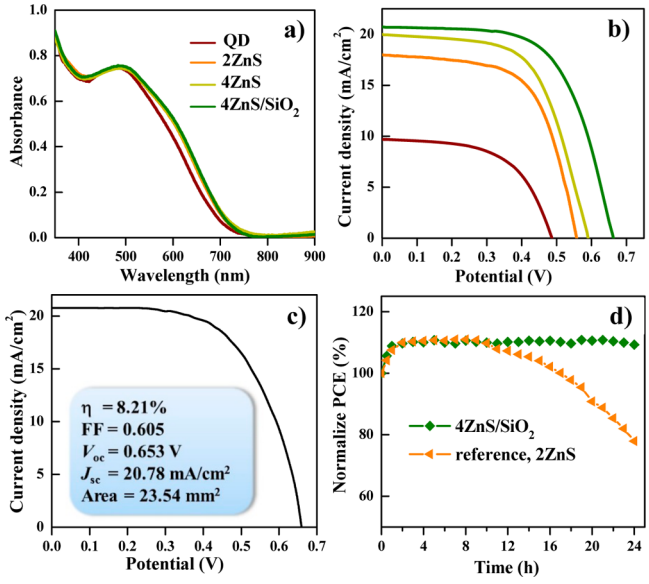

Figure 4. Electrode light absorption and solar cell performance. (a) Absorption spectra of photoanode films after different coatings. (b) *J*–*V* curve of samples prepared with different coatings after QD sensitization. (c) Certified efficiency of QDSC prepared with 4ZnS/SiO_2 coating. (d) Cell efficiency normalized to the initial efficiency for samples with different coating measured during 24 h period under continuous 1 sun illumination.

DOI: 10.1021/jacs.5b01946
J. Am. Chem. Soc. XXXX, XXX, XXX–XXX

Table 1. Photovoltaic Parameters of CdSeTe QDSCs Corresponding to Different Post-Treatment Processes[a]

post-treatment	V_{oc} (V)	J_{sc} (mA/cm^2)	FF (%)	PCE (%)
–	0.473	9.60	55.8	2.53 ± 0.03
2ZnS	0.566 (0.566)	18.02 (18.09)	62.5 (63.0)	6.37 ± 0.05 (6.45)
4ZnS	0.583 (0.591)	19.36 (19.95)	61.4 (60.7)	6.93 ± 0.17 (7.17)
4ZnS/SiO_2	0.656 (0.661)	20.71 (20.73)	61.6 (62.4)	8.37 ± 0.10 (8.55)
4ZnS/SiO_2[b]	0.653	20.78	60.5	8.21

[a]Average solar cell parameters and standard deviations for the seven different device preparations, under 1 sun illumination. The numbers in parentheses represent the values obtained for the champion cells. [b]Certified cell.

Table 2. Average Photovoltaic Parameters and Standard Deviations of Five CdSe QDSCs in Parallel Following Different Post-Treatment Processes

post-treatment[a]	V_{oc} (V)	J_{sc} (mA/cm^2)	FF (%)	PCE (%)[b]
2ZnS, H_2O	0.545 (0.552)	13.49 (13.82)	63.3 (63.3)	4.65 ± 0.14 (4.83)
2ZnS, MeOH	0.550 (0.554)	13.72 (13.80)	66.3 (66.2)	5.01 ± 0.07 (5.07)
4ZnS	0.567 (0.569)	15.57 (15.59)	65.8 (66.3)	5.81 ± 0.06 (5.89)
6ZnS	0.574 (0.576)	15.44 (16.06)	64.8 (64.1)	5.75 ± 0.13 (5.94)
4ZnS/SiO_2	0.620 (0.618)	16.35 (16.57)	65.3 (65.6)	6.62 ± 0.10 (6.71)

[a]MeOH was used in the ZnS post-treatment process if unspecified. The numbers in parentheses represent the values obtained for the champion cells.

assembling these electrodes with Cu_2S/brass foil counter electrodes and polysulfide/sulfide electrolyte (aqueous solution containing 2.0 M Na_2S and S) according to standard literature procedures.[23,48,49] For each cell type, average photovoltaic performance under standard conditions (100 mW/cm^2, AM 1.5G) was analyzed for seven cells in parallel and listed in Table 1, where the results for champion cells obtained for each cell type are also indicated. Current density−voltage (J−V) curves for champion cells are depicted in Figure 4b. The photovoltaic parameters for individual cell are collected in Table S1,2 and Figure S4.

As shown in Figure 4b and Table 1, it is found that QDSCs with inorganic barrier coatings present, in general, higher V_{oc} and J_{sc} than cells processed without further treatments. Furthermore, the nature and thickness of the coating are critical for the photovoltaic performance of the cells. As listed in Tables 1 and S1, it is observed that just 2ZnS coating improves dramatically the cell efficiency by over a factor of 2, while 4ZnS treatment produces a further improvement in photovoltaic performance; from the 6ZnS treatment, the efficiency of the cell decreases gradually. The finding that excessive thick ZnS barrier layer has a negative effect on the performance of the cell can be ascribed to the suppression of hole transfer from the QD to electrolyte. Notably, as predicted by the theoretical analysis, a sequential 4ZnS/SiO_2 coating produces the best results. CdSeTe QDSCs champion cell provided a laboratory PCE of 8.55% with an externally certified efficiency of 8.21% for a cell area of 23.54 mm^2 by the National Center of Supervision and Inspection on Solar Photovoltaic Products Quality of China (CPVT, the detailed information in Figures 4c and S5). This result represents a 38% improvement over the reference cells with a standard post-treatment procedure (2ZnS coating in aqueous media)[36−39] and a 20% enhancement related to previous record-certified efficiency for QDSCs.[11] These results put the QDSC technology at the same efficiency level of depleted heterojunction solar cells,[8−10] but in our case with a considerably larger area.

The small standard deviation from the average value of seven cells as listed in Table 1 indicates that our adopted facile post-treatment process offers excellent performance and high reproducibility for QDSCs. Histograms of cell performance for a larger batch of 200 cell devices shown in Figure S6 further underline the high reproducibility of this approach. Note that, except the synthesis of QDs, all the other fabrication procedures for the construction of QDSCs (such as phase transfer for water-soluble QDs, immobilization of QD on TiO_2 film electrode, overcoating ZnS and SiO_2 on sensitized photoanode, etc.) are all carried out at room temperature and under ambient conditions. This highlights the potential advantage in terms of low-cost and reproducibility for the novel employed QDSC recipe. Furthermore, the reported facile post-treatment process could be generic to QDSCs based on other QD sensitizers. As an example, CdSe-based QDSCs showed an improvement in PCE of 42% by following the 4ZnS/SiO_2 double-layer coating treatment when compared with the regular 2ZnS process. Average photovoltaic performance together with the results of champion cells for each CdSe cell type undergone different post-treatment processes are listed in Table 2. Detailed results for individual cell are depicted in Table S3 and Figure S7.

It is worth commenting that the sequential order of the inorganic layer double coating is critically important to the performance of the resultant cell devices. It is observed that the photovoltaic performance for samples coated with a double layer of SiO_2/4ZnS is poorer than that of 4ZnS/SiO_2 as listed in Table S1. The origin of this difference can be attributed to the different morphology of ZnS and SiO_2 layers. SiO_2 layer presents a high porosity with high micropore volume as indicated in BET measurement with detailed results shown in Figure S8 and Table S4, which allows a good photogenerated hole capture by electrolyte from QD when it covers ZnS in the case of 4ZnS/SiO_2. However, ZnS produces a much more compact coating layer, making the SiO_2/4ZnS combination establish a too thick layer that impedes an adequate QD regeneration.

Furthermore, the stability of the CdSeTe QDSCs undergone 4ZnS/SiO_2 overcoating in the working state was tested in comparison with that of the reference cells after going through the regular 2ZnS treatment using sealed cell configuration,[18] and the results are shown in Figure 4d. As anticipated, the cells

DOI: 10.1021/jacs.5b01946
J. Am. Chem. Soc. XXXX, XXX, XXX−XXX

show better stability after further SiO_2 coating since the thicker ZnS layer combined with further SiO_2 barrier layer prevents photocorrosion reported in chalcogenides under polysulfide and illumination conditions. Experimental results indicate that the PCE values for the reference cells start to decline gradually after 10 h and reach to about 77% of the initial values in a course of 24 h irradiation, while the cells that have undergone $4ZnS/SiO_2$ overcoating process keep nearly the best performance in the course of 24 h irradiation, and then the performance started to decline after ~30 h irradiation.

Although the results shown in Figure 4b are perfectly consistent with the enhanced passivation effect derived by the theory, there are at least three other sources potentially contributing to the experimentally verified improvement of external quantum yield (EQE) as shown in Figure S9: (i) an increase in light harvesting (which can be ruled out, as coating produces a minimum enhancement of light absorption as shown in Figure 4a); (ii) an increase of ET efficiency, and (iii) the enhancement of charge collection efficiency. In order to evaluate these points and to understand the physical origin of the increase of QDSC performance as a function of barrier coatings, terahertz (THz) and impedance spectroscopy (IS) have been carried out.

THz Spectroscopy Characterization. Optical pump THz probe (OPTP) measurements were performed on QD-oxide electrodes for different cell types. All samples analyzed consist on thioglycolic acid (TGA) capped QDs sensitizing a mesoporous TiO_2 film (onto fused silica substrates), followed by different sequential inorganic coating recipes. The OPTP measurements were performed under 400 nm pump (120 $\mu J/cm^2$) and 0.6 THz (2.4 meV) probe conditions; reported traces represent averaged values over 150 scans. OPTP provides a contact-free measurement of the real photoconductivity of the samples following photoexcitation, with subpicosecond (ps) time resolution.[50] OPTP signals in QD-sensitized oxides are only sensitive to free carriers populating the samples, i.e., electrons in the oxide photogenerated from QDs.[51,52] This selectivity allows us to directly quantify ET and recombination dynamics and obtain information about ET yields as a function of postinorganic treatments.[53] Carrier dynamics in the oxide electrode were found to be invariant toward pump fluence up to 160 $\mu J/cm^2$ (see Figure S10a), indicating that electron−electron interactions in the oxide are negligible (even for irradiances well exceeding 1 sun power density). Measurements on up to 8 different spots within each sample recipe show a local variance in photoconductivity of ±8.6% (see Figure S10b), illustrating the homogeneity in electrode sensitization (in good agreement with the narrow distribution of J_{sc}'s obtained for complete devices, see Figure S4). From the comparison of unnormalized amplitudes of the OPTP traces after photoexcitation, and assuming similar QD loadings for all samples tested, we observe that QD-TiO_2 ET efficiencies are not improved for any of the different postinorganic capping treatments (see Figure S10c). In this respect a better passivation of the QDs (increasing the ET efficiency) can be ruled out as a contributor to the increment of the monitored EQE in the devices.

Figure 5a shows the obtained OPTP traces (normalized real conductivity, Re $(\sigma) = \mu \cdot N_e$, where μ refers to the electron mobility, and N_e to the carrier density in the oxide conduction band respectively) as a function of pump−probe delay for the analyzed samples. Concerning the ET rates, the instantaneous emergence of the real conductivity indicates that the ET process taking place from the QD to the oxide is sub-15 ps for all recipes (pump−probe step scan is 15 ps). These ultrafast processes are consistent with the expected strong coupling of the QD sensitizers with the TiO_2 electrode. Assuming that the ET process can be modeled by tunnelling through the barrier imposed by the employed molecular bridge[52] (thioglycolic acid, TGA), the ET rates will be primarily dependent on barrier width and height, donor−acceptor excess energy (ΔG), and the DOS of the oxide acceptor. In previous works we have reported ET rates of ~3 ± 1 ps for CdSe-TGA-SnO_2 (idem linker molecule, ΔG ~1.1 eV and SnO_2 as acceptor). Although in the samples shown in Figure 5a the donor−acceptor ET excess driving energy is reduced ~0.4 eV when compared with our previous findings,[23] the ET rates are expected to be boosted by the increased weight of the DOS of the TiO_2 acceptor when compared with SnO_2 electrodes (note that the TiO_2 (DOS) is ~200-fold bigger when compared with that of SnO_2; this has been correlated with the Ti^{4+} 3d orbital nature of the CB of TiO_2).[54] Following this line of reasoning, it is worth commenting that our findings are in line with the sub-ps dynamics observed in dye-sensitized TiO_2 electrodes[54] and reports on sub-50 fs hot carrier ET for lead salts sensitizing TiO_2 electrodes (even for ΔGs approaching zero).[55,56]

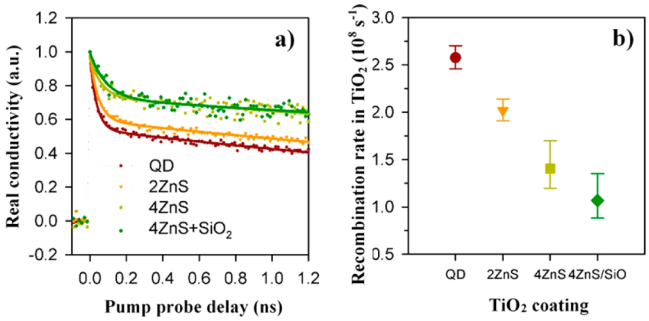

Figure 5. Electrode and device characterization: (a) OPTP traces on CdSeTe QDs sensitizing TiO_2 for different surface inorganic treatments, solid lines are fitting curves using biexponential functions as described in more detail in Supporting Information. (b) Estimated recombination rates as a function of inorganic capping treatment.

The biphasic decay components (Figure 5a) revealed in our time window evidence trapping processes taking place in the oxide electrode. From fitting procedures (shown in Figure S11) we observe that the oxide recombination rates are dependent on capping treatment. Provided that QD/oxide interface (defined by the TGA capping ligand of QD) is preserved independently of postinorganic surface treatment (e.g., donor/acceptor energetics and coupling is identical),[51,52] the monitored changes in recombination should be correlated with enhanced passivation of the TiO_2 surface. Note that recombination processes to the dot should not be affected by the inorganic capping layer, so their influence on the observed trend can be ruled out. Figure 5b presents the estimated recombination rates for the slow component (above 200 ps) as a function of employed coating. The recombination rate in the oxide is reduced following the series: QD > 2ZnS > 4ZnS ≥ $4ZnS/SiO_2$. These results are in good agreement with the theoretical predictions as shown in Figure 1 and device performances as shown in Figure 4. Note that the improved lifetime for the 4ZnS sample when compared with the 2ZnS sample can be attributed to enhanced TiO_2 coverage.

Impedance Spectroscopy Characterization. Impedance spectra (IS) were employed to unveil the intrinsic mechanism

DOI: 10.1021/jacs.5b01946
J. Am. Chem. Soc. XXXX, XXX, XXX−XXX

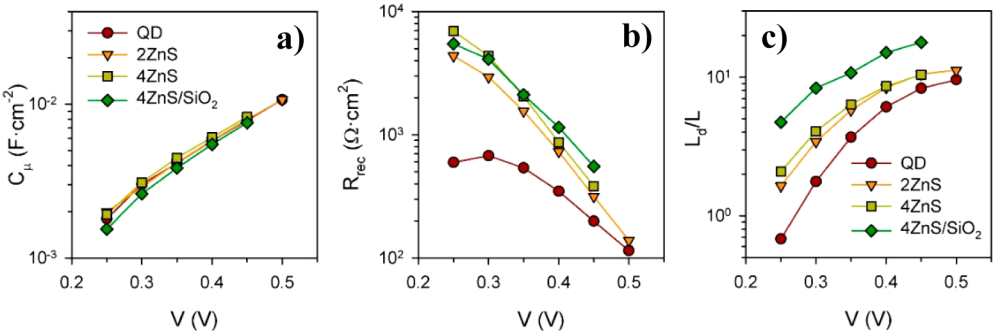

Figure 6. Dependence of (a) chemical capacitance C_μ, (b) recombination resistance R_{rec}, and (c) electron diffusion length L_d of cell samples with different coatings on applied voltage.

of the significantly improved photovoltaic performance of the CdSeTe QDSC after sequential overcoating 4ZnS and SiO_2 on the sensitized photoanodes with use of the standard fitting models for QDSCs.[31,57,58] The detailed Nyquist curves under different bias for 2ZnS, 4ZnS, and 4ZnS + SiO_2 treatment are available in Figure S12. The results reveal that coating does not produce a displacement of the TiO_2 conduction band as no change in the chemical capacitance (C_μ) is observed after coating, as summarized in Figure 6a. This result agrees well with the invariance in ET rates and yields resolved by THz spectroscopy as discussed above. Nevertheless coating has a dramatic effect in recombination resistance, R_{rec}, and in the electron diffusion length, L_d, as summarized in Figure 6b,c, respectively. R_{rec} is reversely proportional to the recombination rate. The introduction of coatings in sensitized photoanode reduces the recombination rate of photogenerated electrons in TiO_2 to accepting species in the electrolyte and therefore brings forward the increase of V_{oc} of the resultant QDSCs,[33] which is also in good agreement with THz characterization (Figure 5b). In addition, coatings also substantially increase L_d, see Figure 6c. This increase of L_d is due to the reduction of R_{rec} as transport resistance, R_{tr}, does not vary with coating, except for the 4ZnS/SiO_2 sample where a decrease is detected, see Figure S13. For samples without coating at low applied bias (close to the short circuit conditions), L_d was lower than the film thickness indicating a poor collection efficiency limiting the photocurrent. Coating increases substantially L_d, obtaining the best results with the double coating. These results confirm that the improvement of cell efficiency with the use of inorganic coatings is obtained via an increase of collection efficiency, which seems to increase with subsequent inorganic treatments as oxide coverage is enhanced and overall passivation increases. As expected, coating layers act as a blocking layer hindering recombination from electrons populating the TiO_2 to holes populating the electrolyte.

CONCLUSIONS

In this paper we demonstrate that a double inorganic coating treatment, consisting on a novel optimized 4ZnS/SiO_2 recipe onto QD-sensitized TiO_2 electrodes, is capable of substantially suppressing recombination losses, boosting PCEs beyond 8%. In addition, we show that the barrier layer post-treatment serves as a protecting shell against QD (and ZnS capping) photocorrosion, enhancing solar cell stability and lifetime. Theory and experiments are able to disentangle the potential contributions to the resolved improvement in solar cell performance. From THz spectroscopy we resolve that the quantum yield and rate of ET from QD to oxide is invariant vs capping architecture. In line with these results, impedance spectroscopy demonstrates that the chemical capacitance is invariant vs the inorganic capping nature, however, collection efficiency is improved by the double inorganic capping when compared with conventional single ZnS treatments. These results illustrate that recombination at the oxide/electrolyte interface is the most sensitive aspect for obtaining improved photovoltage and photocurrent in QDSCs. Furthermore, the presented novel approach is shown to be reproducible, potentially extendable to other QD sensitizers, and provides a path for further development of this low-cost photovoltaic technology.

EXPERIMENTAL SECTION

Electrode and Solar Cell Preparation. TiO_2 nanoparticulate electrodes with 9.0 μm-thick transparent layer and a 6.0 μm-thick light scattering layer over F:SnO_2-coated (FTO, 8 Ω/square) glass substrates were prepared according to literature method.[49] The synthesis and water solubilization of the adopted CdSeTe and CdSe QD sensitizer were according to standard literature procedure.[22,23,48] Transition electron microscopy (TEM) images were obtained using a JEOL JEM-2100 instrument. XPS spectra were conducted under an ESCALAB 250Xi spectrometer. The X-ray source was Al K_α radiation, and the binding energy was calibrated using the C 1s photoelectron peak at 284.6 eV as internal reference. The absorption spectra of QD dispersions and sensitized TiO_2 films (with only transparent layer) were recorded on a UV−vis spectrophotometer (Shimadzu UV-3101 PC). The TiO_2 mesoporous films were sensitized with QD sensitizers by immersing the film in a thioglycolic capped QD aqueous dispersion (with absorbance of 3.0 at 600 nm and pH of 10.0) and staying for 4 h before rinsed sequentially with water and ethanol and then dried with air. After finishing QD sensitizer deposition, the QD bound TiO_2 film was coated with ZnS by dipping alternately into 0.1 M $Zn(OAc)_2$ and Na_2S aqueous solutions for 1 min/dip, rinsing with distilled water between dips. Different numbers of cycles were employed. After coating ZnS layer, further SiO_2 coating was carried out by dipping the ZnS coated photoanodes in 0.01 M tetraethylorthosilicate ethanol solution containing 0.1 M NH_4OH for certain period and then rinsed with water and dried with air. Experimental results indicate that the optimal hydrolysis time of tetraethylorthosilicate is 1 h, which corresponds to the best photovoltaic performance of the resultant cell devices. The cells were prepared by assembling counter electrodes and QD-sensitized photoanodes using a 50 μm thickness scotch spacer and with a droplet (10 μL) of polysulfide electrolyte. The Cu_2S counter electrodes were prepared by immersing brass in HCl solution at 70 °C for 10 min and subsequently dipping it into polysulfide solution for 10 min. The polysulfide electrolyte aqueous solution consists of 2.0 M Na_2S and 2.0 M S. For QDSCs prepared under each condition, seven cells were prepared and tested in parallel.

Photovoltaic Characterization. $J-V$ curves of cell devices were recorded on a Keithley 2400 source meter under illumination by an AM 1.5 G solar simulator (Oriel, model no. 91160, equipped with a

DOI: 10.1021/jacs.5b01946
J. Am. Chem. Soc. XXXX, XXX, XXX−XXX

150 W xenon lamp). The illumination light was calibrated to 100 mW/cm^2 by a NREL standard Si solar cell. Photoactive area of 0.2354 cm^2 was defined by a black mask. EQE spectra were obtained on a Keithley 2000 multimeter under the illumination of a 300 W tungsten lamp with a Spectral Product DK240 monochromator. Impedance spectroscopy measurements were carried out on an impedance analyzer (Zahner, Zennium) in dark conditions at forward bias ranging from 0 V to higher than V_{oc}, applying a 20 mV AC sinusoidal signal over the constant applied bias with the frequency range of 1 MHz to 0.1 Hz.

THz Characterization. A Ti:sapphire amplified laser system (Spitfire ACE by Spectra-Physics) producing ultrashort laser pulses of ~40 fs duration at 800 nm at 1 kHz repetition rate was used to drive the OPTP setup. About 900 mW energy is used to run the optical pump-THz probe spectrometer setup. For the THz generation and detection, 10% of the incoming laser beam is used (90 mW). THz radiation is generated in a phase-matched manner by optical rectification in a ZnTe crystal (⟨110⟩ orientation, 10 × 10 × 1 mm thickness, purchased from MaTeck). The ZnTe generation crystal is pumped with a slightly focused beam (~3 mm diameter) of 800 nm light (80 mW power). The THz light exits the ZnTe generation crystal slightly divergent and is first collimated and subsequently focused on the sample using a pair of off-axis parabolic mirrors. The transmitted THz pulses are recollimated and focused on a second ZnTe detection crystal by another pair of parabolic mirrors, where the instantaneous THz field strength is detected through electro-optical sampling. Optical pump-THz probe spectroscopy for monitoring ET at QD/oxide interfaces was made by selective optical pump of QD sensitizers by a 800 nm femtosecond optical laser pulse and subsequently probing pump induced transient terahertz (2 THz bandwidth) wave absorption with subpicosecond time resolution. In order to prevent any photo-oxidation during the measurements, all samples have been measured under vacuum conditions (1.4 × 10^{-4} mbar).

■ ASSOCIATED CONTENT

Supporting Information

J–*V* curves and photovoltaic parameters of CdSeTe- and CdSe-based cell devices undergone different overcoating treatments. Certified report for photovoltaic performance of CdSeTe cell. Histogram plots of photovoltaic parameters for 200 CdSeTe QDSCs. Nyquist curves and the transport resistance under different bias voltages for CdSeTe cells at forward bias of −0.55 V. Computational methodology, THz characterization, and BET measurements. This material is available free of charge via the Internet at http://pubs.acs.org.

■ AUTHOR INFORMATION

Corresponding Author

*zhongxh@ecust.edu.cn

Author Contributions

#These authors contributed equally.

Notes

The authors declare no competing financial interest.

■ ACKNOWLEDGMENTS

We acknowledge the Natural Science Foundation of China (nos. 21421004, 91433106, 21175043), the Science and Technology Commission of Shanghai Municipality (nos. 11JC1403100, 12NM0504101), the Fundamental Research Funds for the Central Universities in China, and the Max Planck Society and Universitat Jaume I project 12I361.01/1 for financial support. H.W. is a recipient of a fellowship of the Graduate School Materials Science in Mainz funded through the German Research Foundation in the Excellence Initiative (GSC 266).

■ REFERENCES

(1) Swierk, J. R.; Mallouk, T. E. *Chem. Soc. Rev.* **2013**, *42*, 2357–2387.
(2) Sargent, E. H. *Nat. Photonics* **2012**, *6*, 133–135.
(3) Kamat, P. V. *Acc. Chem. Res.* **2012**, *45*, 1906–1915.
(4) Kramer, I. J.; Sargent, E. H. *Chem. Rev.* **2014**, *114*, 863–882.
(5) Nozik, A. J.; Beard, M. C.; Luther, J. M.; Law, M.; Ellingson, R. J.; Johnson, J. C. *Chem. Rev.* **2010**, *110*, 6873–6890.
(6) Semonin, O. E.; Luther, J. M.; Choi, S.; Chen, H.-Y.; Gao, J.; Nozik, A. J.; Beard, M. C. *Science* **2011**, *334*, 1530–1533.
(7) Hodes, G. *J. Phys. Chem. C* **2008**, *112*, 17778–17787.
(8) Chuang, C. M.; Brown, P. R.; Bulovic, V.; Bawendi, M. G. *Nat. Mater.* **2014**, *13*, 796–801.
(9) Ip, A. H.; Thon, S. M.; Hoogland, S.; Voznyy, O.; Zhitomirsky, D.; Debnath, R.; Levina, L.; Rollny, L. R.; Carey, G. H.; Fischer, A.; Kemp, K. W.; Kramer, I. J.; Ning, Z.; Labelle, A. J.; Chou, K. W.; Amassian, A.; Sargent, E. H. *Nat. Nanotechnol.* **2012**, *7*, 577–582.
(10) Ning, Z.; Voznyy, O.; Pan, J.; Hoogland, S.; Adinolfi, V.; Xu, J.; Li, M.; Kirmani, A. R.; Sun, J.-P.; Minor, J.; Kemp, K. W.; Dong, H.; Rollny, L.; Labelle, A.; Carey, G.; Sutherland, B.; Hill, I.; Amassian, A.; Liu, H.; Tang, J.; Bakr, O. M.; Sargent, E. H. *Nat. Mater.* **2014**, *13*, 822–828.
(11) Jiao, S.; Shen, Q.; Mora-Seró, I.; Wang, J.; Pan, Z.; Zhao, K.; Kuga, Y.; Zhong, X.; Bisquert, J. *ACS Nano* **2015**, *9*, 908–915.
(12) Ruhle, S.; Shalom, M.; Zaban, A. *ChemPhysChem* **2010**, *11*, 2290–2304.
(13) Kamat, P. V.; Tvrdy, K.; Baker, D. R.; Radich, J. G. *Chem. Rev.* **2010**, *110*, 6664–6688.
(14) Choi, Y. C.; Lee, D. U.; Noh, J. H.; Kim, E. K.; Seok, S. I. *Adv. Funct. Mater.* **2014**, *24*, 3587–3592.
(15) Giménez, S.; Mora-Seró, I.; Macor, L.; Guijarro, N.; Lana-Villarreal, T.; Gómez, R.; Diguna, L. J.; Shen, Q.; Toyoda, T.; Bisquert, J. *Nanotechnology* **2009**, *20*, 295204.
(16) Radich, J. G.; Dwyer, R.; Kamat, P. V. *J. Phys. Chem. Lett.* **2011**, *2*, 2453–2460.
(17) Lin, C. Y.; Teng, C. Y.; Li, T. L.; Lee, Y. L.; Teng, H. S. *J. Mater. Chem. A* **2013**, *1*, 1155–1162.
(18) Zhao, K.; Yu, H.; Zhang, H.; Zhong, X. *J. Phys. Chem. C* **2014**, *118*, 5683–5690.
(19) Jiang, Y.; Zhang, X.; Ge, Q.; Yu, B.; Zou, Y.; Jiang, W.; Song, W.; Wan, L.; Hu, J. *Nano Lett.* **2014**, *14*, 365–372.
(20) Wang, J.; Mora-Sero, I.; Pan, Z. X.; Zhao, K.; Zhang, H.; Feng, Y.; Yang, G.; Zhong, X. H.; Bisquert, J. *J. Am. Chem. Soc.* **2013**, *135*, 15913–15922.
(21) Yan, K. Y.; Zhang, L. X.; Qiu, J. H.; Qiu, Y. C.; Zhu, Z. L.; Wang, J. N.; Yang, S. H. *J. Am. Chem. Soc.* **2013**, *135*, 9531–9539.
(22) Zhang, H.; Cheng, K.; Hou, Y.; Fang, Z.; Pan, Z. X.; Wu, W. J.; Hua, J. L.; Zhong, X. H. *Chem. Commun.* **2012**, *48*, 11235–11237.
(23) Pan, Z.; Zhao, K.; Wang, J.; Zhang, H.; Feng, Y. Y.; Zhong, X. H. *ACS Nano* **2013**, *7*, 5215–5222.
(24) Lee, J.-W.; Son, D.-Y.; Ahn, T. K.; Shin, H.-W.; Kim, I. Y.; Hwang, S.-J.; Ko, M. J.; Sul, S.; Han, H.; Park, N.-G. *Sci. Rep.* **2013**, *3*, 1050.
(25) Li, W.; Zhong, X. *J. Phys. Chem. Lett.* **2015**, *6*, 796–806.
(26) Kamat, P. V. *J. Phys. Chem. Lett.* **2013**, *4*, 908–918.
(27) Li, L.; Yang, X.; Gao, J.; Tian, H.; Zhao, J.; Hagfeldt, A.; Sun, L. *J. Am. Chem. Soc.* **2011**, *133*, 8458–8460.
(28) Pan, Z. X.; Mora-Seró, I.; Shen, Q.; Zhang, H.; Li, Y.; Zhao, K.; Wang, J.; Zhong, X. H.; Bisquert, J. *J. Am. Chem. Soc.* **2014**, *136*, 9203–9210.
(29) McDaniel, H.; Fuke, N.; Makarov, N. S.; Pietryga, J. M.; Klimov, V. I. *Nat. Commun.* **2013**, *4*, 2887.
(30) Hagfeldt, A.; Boschloo, G.; Sun, L.; Kloo, L.; Pettersson, H. *Chem. Rev.* **2010**, *110*, 6595–6663.
(31) Mora-Seró, I.; Gimenez, S.; Fabregat-Santiago, F.; Gomez, R.; Shen, Q.; Toyoda, T.; Bisquert, J. *Acc. Chem. Res.* **2009**, *42*, 1848–1857.
(32) Palomares, E.; Clifford, J. N.; Haque, S. A.; Lutz, T.; Durrant, J. R. *J. Am. Chem. Soc.* **2003**, *125*, 475–482.

DOI: 10.1021/jacs.5b01946
J. Am. Chem. Soc. XXXX, XXX, XXX–XXX

(33) Chandiran, A. K.; Nazeeruddin, M. K.; Graetzel, M. *Adv. Funct. Mater.* **2013**, *24*, 1615−1623.
(34) Prasittichai, C.; Avila, J. R.; Farha, O. K.; Hupp, J. T. *J. Am. Chem. Soc.* **2013**, *135*, 16328−16331.
(35) Son, H.-J.; Wang, X.; Prasittichai, C.; Jeong, N. C.; Aaltonen, T.; Gordon, R. G.; Hupp, J. T. *J. Am. Chem. Soc.* **2012**, *134*, 9537−9540.
(36) Yang, S.; Huang, C.; Zhai, J.; Wang, Z.; Jiang, L. *J. Mater. Chem.* **2002**, *12*, 1459−1464.
(37) Diguna, L. J.; Shen, Q.; Kobayashi, J.; Toyoda, T. *Appl. Phys. Lett.* **2007**, *91*, 023116.
(38) Hachiya, S.; Shen, Q.; Toyoda, T. *J. Appl. Phys.* **2008**, *103*, 084304.
(39) Guijarro, N.; Campina, J. M.; Shen, Q.; Toyoda, T.; Lana-Villarreala, T.; Gomez, R. *Phys. Chem. Chem. Phys.* **2011**, *13*, 12024−12032.
(40) Shalom, M.; Dor, S.; Ruhle, S.; Grinis, L.; Zaban, A. *J. Phys. Chem. C* **2009**, *113*, 3895−3898.
(41) Roelofs, K. E.; Brennan, T. P.; Dominguez, J. C.; Bailie, C. D.; Margulis, G. Y.; Hoke, E. T.; McGehee, M. D.; Bent, S. F. *J. Phys. Chem. C* **2013**, *117*, 5584−5592.
(42) Liu, Z.; Miyauchi, M.; Uemura, Y.; Cui, Y.; Hara, K.; Zhao, Z.; Sunahara, K.; Furube, A. *Appl. Phys. Lett.* **2010**, *96*, 233107.
(43) Tachan, Z.; Hod, I.; Shalom, M.; Grinis, L.; Zaban, A. *Phys. Chem. Chem. Phys.* **2013**, *15*, 3841−3845.
(44) Barea, E. M.; Shalom, M.; Gimenez, S.; Hod, I.; Mora-Seró, I.; Zaban, A.; Bisquert, J. *J. Am. Chem. Soc.* **2010**, *132*, 6834−6839.
(45) de la Fuente, M. S.; Sánchez, R. S.; González-Pedro, V.; Boix, P. P.; Mhaisalkar, S. G.; Rincón, M. E.; Bisquert, J.; Mora-Seró, I. *J. Phys. Chem. Lett.* **2013**, *4*, 1519−1525.
(46) Meng, Q.; Wang, T.; Liu, E.; Ma, X.; Ge, Q.; Gong, J. *Phys. Chem. Chem. Phys.* **2013**, *15*, 9549−9561.
(47) Perdew, J. P.; Burk, K.; Ernzerhof, M. *Phys. Rev. Lett.* **1996**, *77*, 3865−3868.
(48) Yang, J. W.; Oshima, T.; Oshima, W.; Pan, Z. X.; Zhong, X. H.; Shen, Q. *J. Mater. Chem. A* **2014**, *2*, 20882−20888.
(49) Du, Z.; Zhang, H.; Bao, H.; Zhong, X. *J. Mater. Chem. A* **2014**, *2*, 13033−13040.
(50) Ulbricht, R.; Hendry, E.; Shan, J.; Heinz, T. F.; Bonn, M. *Rev. Mod. Phys.* **2011**, *83*, 543−586.
(51) Cánovas, E.; Moll, P.; Jensen, S. A.; Gao, Y.; Houtepen, A. J.; Siebbeles, L. D. A.; Kinge, S.; Bonn, M. *Nano Lett.* **2011**, *11*, 5234−5239.
(52) Wang, H.; McNellis, E. R.; Kinge, S.; Bonn, M.; Cánovas, E. *Nano Lett.* **2013**, *13*, 5311−5315.
(53) Wang, H.; Barceló, I.; Lana-Villarreal, T.; Gómez, R.; Bonn, M.; Cánovas, E. *Nano Lett.* **2014**, *14*, 5780−5786.
(54) Asbury, J. B.; Hao, E.; Wang, Y.; Ghosh, H. N.; Lian, T. *J. Phys. Chem. B* **2001**, *105*, 4545−4557.
(55) Tisdale, W. A.; Williams, K. J.; Timp, B. A.; Norris, D. J.; Aydil, E. S.; Zhu, X.-Y. *Science* **2010**, *328*, 1543−1547.
(56) Yang, Y.; Rodríguez-Córdoba, W.; Xiang, Xu.; Lian, T. *Nano Lett.* **2012**, *12*, 303−309.
(57) González-Pedro, V.; Xu, X.; Mora-Seró, I.; Bisquert, J. *ACS Nano* **2010**, *4*, 5783−5790.
(58) Fabregat-Santiago, F.; Garcia-Belmonte, G.; Mora-Seró, I.; Bisquert, J. *Phys. Chem. Chem. Phys.* **2011**, *13*, 9083−9118.

DOI: 10.1021/jacs.5b01946
J. Am. Chem. Soc. XXXX, XXX, XXX−XXX